75th International Astronautical Congress (IAC), Milan, Italy, 14-18 October 2024.

IAC–24–C1.6.3

ANIME Asteroid CubeSat Mission Concept and Rendezvous Phase: Progressive Hyperbolic Arcs Design for Radio-Science and Close Observation

Enrico Belloni[a]*, **Fabrizio Maccari**[a], **Michèle Lavagna**[a]

[a] *Department of Aerospace Science and Technology, Politecnico di Milano, Italy*

* Corresponding Author: enrico.belloni@polimi.it

Over recent years, there has been a growing emphasis on planetary defense missions aimed at investigating small celestial bodies that pose potential collision risks with Earth. ANIME is a 12U CubeSat mission currently in Phase A having as objective a rendezvous with asteroid 2000 SG344, the largest object known to have a better than 0.1% of impacting Earth. The scientific objective is to explore the target to collect far and close-range measurements via two optical payloads and performing several radio-science measurements. During its interplanetary travel towards its final destination, ANIME will also fly by two additional potentially hazardous asteroids, still to be defined, in order to collect additional measurements of NEA objects. The proximity trajectory design after rendezvous with 2000 SG344 is driven by the imaging and radio-science requirements selected by the scientific team. The proposed strategy manages to satisfy the scientific requests while exploiting the natural dynamics of the system to minimize fuel consumption, a critical aspect for the very limited resources of a 12U CubeSat mounting only an electric propulsion unit. The design starts from the definition of progressively approaching hyperbolic arcs and station keeping maneuvers via a single shooting optimization algorithm with impulsive approximation of the thrusting arcs. Then, the trajectory of the entire phase is refined by removing the impulsive assumption computing the corresponding low thrust control profiles with Sequential Convex Programming techniques. The trajectory output is then used as reference and numerically tested in several Monte Carlo analyses with a high-fidelity orbital propagator including expected uncertainty sources deriving from the platform and the poorly known environment. The results demonstrate that the designed strategy satisfies all the scientific requirements for imaging and radio-science while still complying with the stringent constraints given by the platform, allowing to state the feasibility of the ANIME deep space CubeSat mission concept.

Keywords: ANIME, 2000 SG344, Trajectory design, Model Predictive Control, Sequential Convex Programming

Nomenclature

$\mathbf{A}$	: dynamics plant matrix
a	: semi-major axis
$\mathbf{B}$	: control input matrix
e	: eccentricity
J	: cost functional
G	: universal gravity constant
g	: gravitational acceleration
m	: mass
$\underline{\mathbf{r}}$	: position vector
T	: engine thrust
t	: time
$\underline{\mathbf{u}}$	: control vector
$\underline{\mathbf{x}}$	: state vector
μ	: gravitational parameter

Abbreviations

CR3BP	: circular restricted three-body problem
GNC	: guidance, navigation and control
KOZ	: Keep Out Zone
LOS	: Line of Sight
MC	: Monte Carlo
MPC	: model predictive control
NEA	: Near Earth Asteroid
SCP	: Sequential Convex Programming
SPA	: Sun-Phase-Angle
SRP	: Solar Radiation Pressure
ToF	: time of flight
ZOH	: Zero-Order-Hold

1. Introduction

The possibility of using CubeSats for interplanetary missions has emerged as a prominent opportunity for the next years of space exploration, as shown by the successful precedents set by MarCO (NASA) [1], LICIACube (ASI) [2], and the upcoming Juventas (ESA) [3] and Milani (ESA) [4]. Nanosatellites may indeed provide a cost-effective solution to complement larger conventional spacecraft, augmenting the scientific return while providing in-orbit demonstration of disruptive technologies. The ANIME mission is a 12U CubeSat that will fly by two different Near Earth Asteroids before performing a rendezvous for scientific operations with a third target, 2000 SG344. The study is the effort of a consortium led by INAF OAR, including Politecnico di Milano, INAF OAPd, Politecnico di Torino and Università di Bologna and it has recently completed Phase A, as part of the ALCOR program financed by ASI. The mission is currently foreseen for launch in a window spanning from late 2029 to 2033 and will embark on a 2-year interplanetary transfer using a low-thrust electric propulsion unit, that will be also used for proximity maneuvering. Then, 2 months of scientific operations are foreseen, following the trajectory that is presented and detailed in this paper. The study has the goal to gain new insights on the formation process and composition of potentially hazardous near-earth asteroids of small dimensions. The scientific return of the mission will be provided by the images taken by two cameras, a far range and a close range imager, and will also be complemented by radio-science experiments.

Designing proximity operations for a CubeSat around 2000 SG344 is particularly challenging because the target is very small, with an estimated diameter of 40m, a largely uncertain estimated mass of $7 \cdot 10^7$ kg [5], and an unknown shape. The resulting gravitational pull is therefore limited, and active control is required to stay in proximity of the target. Moreover the design of the operations has to be robust, complying with the scientific requirements in a large span of possible conditions. Additionally, the platform has limited onboard resources, both in terms of control authority and of computational power.

The proposed strategy starts from the definition of progressively approaching hyperbolic arcs with the assumption of impulsive maneuvers, performed according to an averaged lower fidelity model that holds throughout an entire year, to maintain flexibility with respect to the actual launch date. Once a nominal first trajectory is retrieved, it is used as baseline to generate the low-thrust counterpart, which is computed exploiting a Sequential Convex Programming algorithm [6] starting from actual initial and environmental conditions and propagated using a high-fidelity propagator. Montecarlo simulations are then performed with the convex optimizer in closed loop to check for the robustness of the proposed trajectories to the extremely wide range of uncertainties at this early stage of the design, verifying that the trajectory is controllable and that the desired scientific objectives can be satisfied irrespectively of the departure date.

2. System dynamics

Two dynamical formulations have been used to carry out the work presented in the following: as anticipated, a simplified model is used to design the nominal trajectory, whereas a higher fidelity model is introduced to validate the trajectory design and the computed guidance law in a more realistic scenario.

2.1 Simplified Model

The motion of a particle in the vicinity of an asteroid can be described with the equations of the classical circular restricted three-body problem (CR3BP), where the spacecraft is assumed to move under the gravitational influence of the Sun and the asteroid. In addition, due to the small mass ratio and satellite distance to the target surface, the system is also suitable for Circular Hill's approximation [7]. In fact, the eccentricity of the orbit of the asteroid around the Sun is very low and in any case, it can be neglected for this analysis due to the short time scale of the maneuvers. The equations of motion are defined in a rotating reference frame located at the center of mass of 2000 SG344, where the x axis is parallel to the line connecting the two bodies and pointing towards the Sun, the z axis is parallel to the orbit angular momentum vector of the asteroid, and the y axis completes the right-handed triad. The acceleration due to the Solar Radiation Pressure (SRP) is also added to the model, according to the simplified formulation in [7], clearly directed along the x axis of the reference frame:

$$a_{srp} = \frac{(1+\rho)G_1 A/m}{d^2} \tag{1}$$

In which ρ is the spacecraft reflectance coefficient (assumed to be equal to 0.8), $G_1 = 10^8$ kg·km^3/s^2/m^2 is the expected radiation flux, A/m is the area to mass ratio of the spacecraft, and d is taken as the average distance of the asteroid from the sun. The equations of motion in the Hill's reference frame therefore read:

$$\dot{\mathbf{v}} = -\frac{\mu}{r^3}\mathbf{r} + 2n \begin{bmatrix} v_y \\ -v_x \\ 0 \end{bmatrix} + n^2 \begin{bmatrix} 3x \\ 0 \\ -z \end{bmatrix} + a_{srp} \begin{bmatrix} 1 \\ 0 \\ 0 \end{bmatrix} \tag{2}$$

Where n is the mean motion of the asteroid around the sun, r the distance between the asteroid and the spacecraft, and xyz are the position coordinates in the Hill reference frame.

2.2 Higher Fidelity Model

The higher fidelity model has the purpose to more accurately describe the motion of the asteroid and of the spacecraft around the sun during the propagation, including a dependence on the departure date. Indeed, the asteroid and the spacecraft are both propagated in the ECLIPJ2000 frame, in an ephemeris-based n-body propagator. The bodies considered as attractors in the model are the ones known to be the most relevant for NEAs: Sun, Earth and Moon. The ephemeris of the bodies are recovered with the SPICE toolkit [8], from the DE432s kernel. The initial conditions of the asteroid are retrieved at the initial time of the propagation from the SPICE kernel provided by the NASA JPL horizons database [9].
The asteroid gravitational attraction and the SRP, computed as in eq. (1), are also considered in the spacecraft's dynamics. After the propagation, the spacecraft state in ECLIPJ2000 coordinates can then be transformed in the corresponding $\mathbf{r}, \mathbf{v}$ vectors in the Hill's reference frame.

3. Nominal Trajectory Design

The nominal trajectory is designed selecting a sequence of progressively approaching hyperbolic arcs with the aim to satisfy the scientific requirements of the mission. Images shall be acquired at different resolution levels (0.5 m, 0.25 m, 0.1 m and 0.05 m) and in a wide range of Sun-Phase-Angle (SPA) ($40^\circ - 60^\circ$ at the lower resolutions, $0^\circ - 150^\circ$ at the higher ones). Knowing the characteristics of the embarked optical payloads, the resolution requirements have been translated into holding distances from the target, at which the imaging shall occur. In addition, the mission aims also to perform radioscience experiments, with low velocity and low distance passages near 2000 SG344.
To satisfy all the previous requirements, the rendezvous phase of the mission is split in the following sub-phases: Far Range Operations, Close Range Operations and disposal. In all the sub-phases, the arcs have been designed selecting the initial and final conditions looking at the requirements and then performing single-shooting optimization to find the trajectory that minimizes the required ΔV of the maneuvers according to an impulsive simplification of the problem. The duration of the arcs, t_{arc} is a parameter to be defined in the design phase, according to operational constraints regarding telecommunication windows.
Maneuvers have been approximated as impulsive firings for the nominal trajectory design, one happening at the beginning of the arc, $\Delta\mathbf{v}_0$, and one at the end, $\Delta\mathbf{v}_\mathrm{f}$. The components of these two vectors are the design variables of the single shooting problem, defined for each arc as:

$$\begin{aligned} &\min_{\Delta\mathbf{v}_0, \Delta\mathbf{v}_\mathrm{f} \in [-\Delta V_{max}, \Delta V_{max}]} \Delta V = \|\Delta\mathbf{v}_0\| + \|\Delta\mathbf{v}_\mathrm{f}\| \\ &\text{subject to:} \\ &\phi(\mathbf{x}_0, t_{arc}) + [\mathbf{0}_{1x3}, \Delta\mathbf{v}_\mathrm{f}^T]^T - \mathbf{x}_T = 0 \end{aligned} \tag{3}$$

The initial state $\mathbf{x}_0$ is defined as the vector $\mathbf{x}_0 = [\mathbf{r}_0, \mathbf{v}_0 + \Delta\mathbf{v}_0]$, with the initial conditions $\mathbf{r}_0$, $\mathbf{v}_0$ that are selected a priori, as well as the target state $\mathbf{x}_T$ at the end of each arc. The constraint enforces the matching between the final point of the propagation of $\mathbf{x}_0$ and the target state $\mathbf{x}_T$, before the final burn.
The domain of feasibility is instead introduced to bound the search space limiting the maximum firing time to one hour, from which a ΔV_{max} is derived.
The impulsive manoeuvres approximation will be removed to compute the actual low-thrust guidance profile of the mission, as detailed in section 4.

3.1 Far Range Operations

The far range trajectory, represented in its entirety in fig. 1, is organised in sequences of multiple observation arcs at three holding distances at 50 km, 25 km, and 10 km, which are followed by a transfer towards the close range.

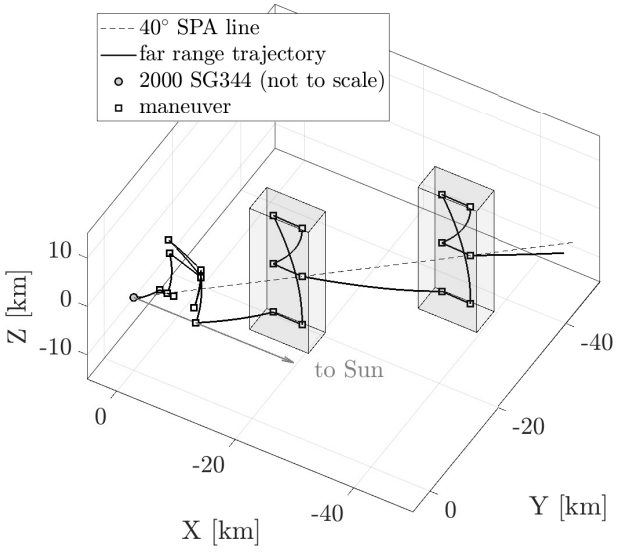

Fig. 1: Far Range nominal trajectory evolution in the Hill's reference frame.

The trajectory is designed trying to exploit as much as possible the dynamics of the environment, to optimize the utilization of the limited propellant resources of the platform. Indeed, at the first two holding distances, the implemented station keeping strategy leverages the solar radiation pressure to make the spacecraft drift inside a box, designed considering the constraints on the sun phase angle and allowing the out-of-plane imaging of the asteroid, to increase the possibility of observing the poles. The boxes are designed along an approach line at 40° SPA, to exploit then the solar radiation pressure to drift to higher values of Sun-Phase angle, towards the maximum desired threshold of 60°. Each arc has a nominal duration of 2.5 days in order to leave enough time for scientific acquisition while also avoid congestion of the ground segment due to excessively frequent communication when not needed. The last far range observation arcs are instead designed ad-hoc at a 10km holding distance, to cover a wider range of SPA, as required by the science team. The first three arcs in this phase have a duration of 1.5 days, while the latter 4 have a duration of 1 day. The evolution in time of SPA and distance from 2000 SG344 is shown fig. 2, underlining the compliance with the requirements. The far range trajectory finally ends with the transfer towards the close range, split in two by arcs at an holding distance of 5 km, to ensure enough time to study the shape and dynamics of the asteroid before transitioning to the shorter distances. The overall impulsive ΔV for the far range phase is 2.91 m/s, with a time of flight of 40.5 days.

3.2 Close Range Operations

During the close range operations, in addition to the resolution and SPA requirements, the radio-science requirements come into play as well, adding additional constraints to the design of the orbital trajectory. More in detail, close passages shall take place at a distance from the target lower than 1 km while maintaining a velocity of the spacecraft lower than 2.5 times the escape velocity of the system. In addition, it must also be taken into account that at distances below 400 m from the target, the close range imager to be used in this phase starts going out of focus. To satisfy all these requirements, the trajectory presented in fig. 3 is proposed. The design consists in nine hyperbolic arcs of one day of duration, starting from the arrival point from the far range and ending at the starting point of the disposal operations. The evolution of the distance from the center of mass of the target is shown in fig. 4 together with the Sun-Phase Angles seen by the spacecraft during this phase. It can be noticed that the target remains always in the ideal distance range for imaging, while also crossing the full range of SPA of interest. Lastly, fig. 5 shows that the escape velocity requirement is satisfied for the majority of the trajectory, far from the maneuvering points. The duration of the close-range operations is of 9 days, with a computed impulsive ΔV of 0.34 m/s. After the close range operations the CubeSat will perform a disposal transfer, ending with an impact with a reduced speed with the target. The nominal disposal trajectory consists in a last bi-impulsive arc towards a point

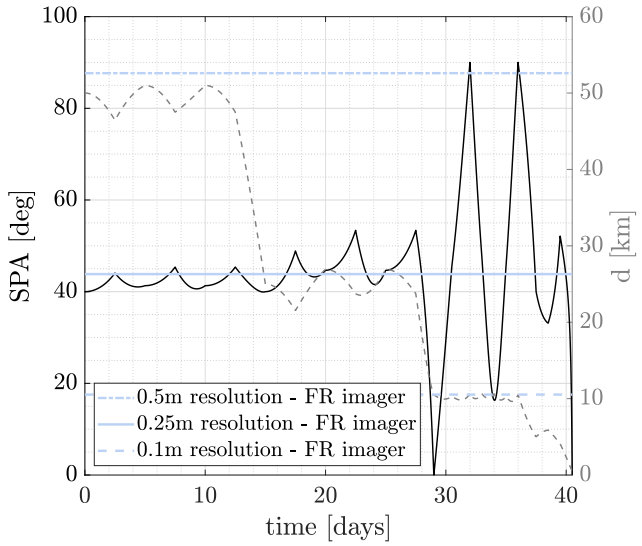

Fig. 2: Sun-Phase Angle and distance evolution during Far Range operations.

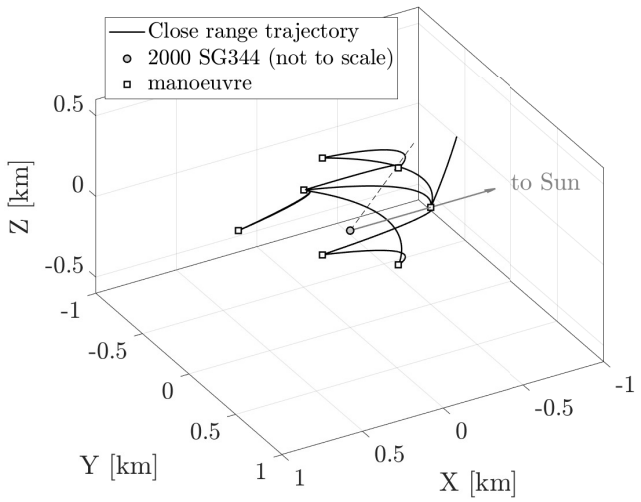

Fig. 3: Close Range nominal trajectory evolution in the Hill's reference frame.

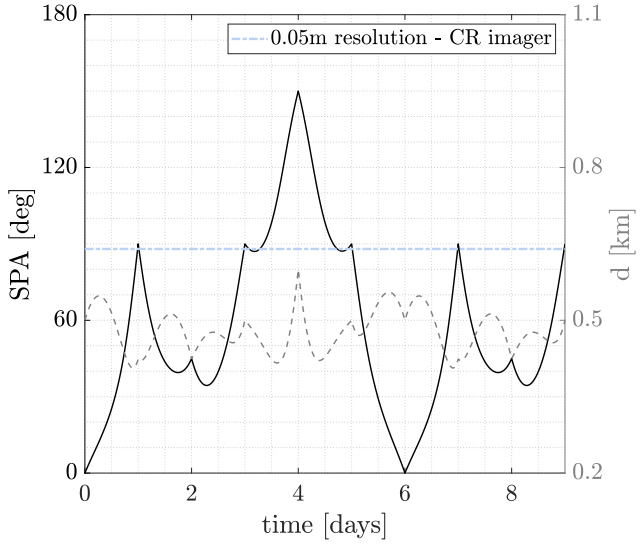

Fig. 4: Sun-Phase Angle and distance evolution during Close Range operations.

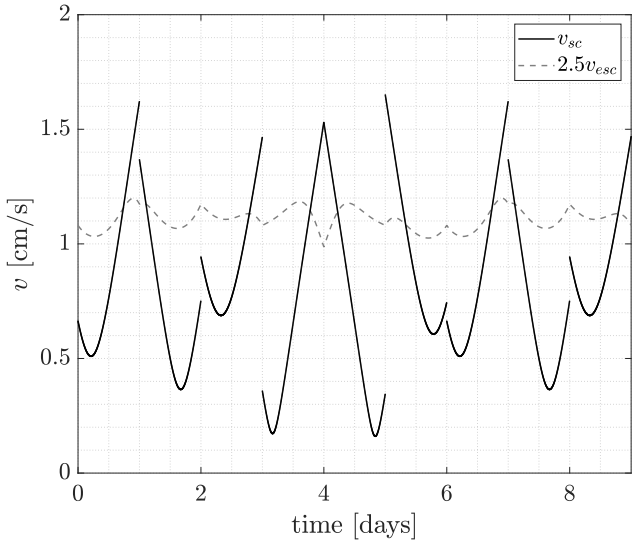

Fig. 5: Velocity evolution during close range operations, compared to radio-science requirement.

in front of the target with respect to the sun, before leaving the spacecraft to drift towards the asteroid thanks to the effect of the SRP.

4. Low-thrust guidance generation

As previously introduced, the reference trajectory is computed starting from averaging assumptions to cover the wide range of departure dates that is envisioned for the ANIME mission to guarantee the requested flexibility. In order to remove the impulsive assumption and still follow closely the planned trajectory considering the range of uncertainties if such problem, a receding horizon guidance update strategy is used to recompute the optimal trajectory of each arc taking into account the measured state and constraints differences with respect to the expected nominal values. In order to obtain a computationally efficient solution that could be potentially even be run onboard, the problem is formulated in the context of constrained optimal convex optimization framework. More in detail, due to the presence of nonlinear dynamics constraint and a nonconvex spherical keep-out zone, Sequential Convex Programming (SCP) techniques are used to provide an iterative framework in which the problem is solved via a sequence of convex subproblems. The selected SCP technique is Guaranteed Sequential Trajectory Optimization (GuSTO), a SCP trust region algorithm which finds its theoretical convergence proof in the Pontryagin Maximum Principle for which the entire implementation can be found in [6]. Hereafter, the problem-specific formulation is described.

4.1 OCP cost function

The specific implementation of GuSTO is designed to handle artificial unboundedness by augmenting the cost function with a soft penalty on the violation of a trust region and to avoid artificial infeasibility by augmenting the problem cost function with a penalty on the violation of non-convex path constraints. The original cost function is in fact just the weighted sum of a quadratic term in the control variable and the time of flight of the arc that is being optimized:

$$\Gamma(\mathbf{u}, p) = \frac{1}{2}\mathbf{u}^{\mathrm{T}} Q \mathbf{u} + w \cdot t_f \tag{4}$$

The soft penalties are then included via a convex and non-decreasing penalty function $h_\lambda : \mathbb{R} \to \mathbb{R}_+$ that depends on a scalar weight λ. The goal of is to penalize any positive value while being agnostic to non-positive values. The formulation chosen for the application of this paper is to simply take the positive part of the argument:

$$h_\lambda(\mathbf{z}) = \lambda([\mathbf{z}]^+) \tag{5}$$

Hence, the soft penalty on the non-convex path constraint violation can be expressed as:

$$g_{pc}(\mathbf{x}, p) \triangleq h_\lambda(s(\mathbf{x}, p)) \tag{6}$$

Where $s(\mathbf{x}, p)$ is the function that defines the nonconvex path contraint:

$$s(\mathbf{x},p) \triangleq R_{\text{koz}}^2 - \mathbf{r}(t)\cdot\mathbf{r}(t) \leq 0 \tag{7}$$

In order to convexify the nonconvex expression, the following Jacobians are defined:

$$\hat{C} = \nabla_x s(\bar{\mathbf{x}},\bar{p}) \tag{8a}$$
$$\hat{G} = \nabla_p s(\bar{\mathbf{x}},\bar{p}) \tag{8b}$$

So that the convex approximation of $g_{pc}(\mathbf{x},p)$ can be expressed as:

$$\breve{g}_{pc}(\mathbf{x},p) = h_\lambda(s(\bar{\mathbf{x}},\bar{p}) + \hat{C}\delta\mathbf{x} + \hat{G}\delta p) \tag{9}$$

On the other hand, the term penalizing trust region violation to limit artificial unboundedness is added as:

$$g_{tr}(\mathbf{x},p) \triangleq h_\lambda(\|\delta\mathbf{x}(t)\|_q + \|\delta p\|_q - \eta) \tag{10}$$

where $q \in \{1,2,\infty\}$ defines the norm type of choice and $(\delta\mathbf{x}(t),\ \delta p)$ define the variation of the state and the parameters between two consecutive iterations of the SCP algorithm. Now the full convex expression of the OCP cost function can be written by integrating in the $[0,1]$ time interval as:

$$L_\lambda(\mathbf{x},\mathbf{u},p) = \int_0^1 \Gamma(\mathbf{u},p) + \breve{g}_{pc}(\mathbf{x},p) + g_{tr}(\mathbf{x},p) \tag{11}$$

To be able to the derived cost functional it in a direct optimization framework, the solution must be expressed according to the selected time discretization dividing the $[0,1]$ interval into N samples. This is achieved by substituting the continuous time integrals with their discrete approximation:

$$\int_0^1 z\,dt \approx \Delta t \sum_{k=1}^{N} z_k \tag{12}$$

where:

$$\Delta t = \frac{1}{N-1} \tag{13}$$

4.2 Dynamics formulation

The following step in constructing a convex optimal control problem is to obtain a suitable formulation for the dynamics expression. The equations of motion of the system in Equation 2 can be re-formulated in linear state-space form including an input control action $\underline{\mathbf{u}}$ as:

$$f(\mathbf{x},\mathbf{u}) = \mathbf{A}\underline{\mathbf{x}}(t) + \mathbf{B}(\underline{\mathbf{u}}(t) + \underline{\mathbf{g}}(t) + \underline{\mathbf{a}}_{\mathbf{srp}}) \tag{14}$$

defined in the $[0,1]$ time interval. Then, to define the problem with free final time, the parameter p is introduced to rescale the time interval to $\mathrm{t} \in [0,t_f]$ by defining the time dilation $\mathrm{t} = pt$:

$$f(\mathbf{x},\mathbf{u},p) = pf(\mathbf{x},\mathbf{u}) \tag{15}$$

in which the plant and control matrices are expressed as:

$$\mathbf{A} = \begin{bmatrix} 0 & 0 & 0 & 1 & 0 & 0 \\ 0 & 0 & 0 & 0 & 1 & 0 \\ 0 & 0 & 0 & 0 & 0 & 1 \\ 3 & 0 & 0 & 0 & 2 & 0 \\ 0 & 0 & 0 & -2 & 0 & 0 \\ 0 & 0 & -1 & 0 & 0 & 0 \end{bmatrix} \tag{16}$$

$$\mathbf{B} = \begin{bmatrix} 1 & 0 & 0 \\ 0 & 1 & 0 \\ 0 & 0 & 1 \end{bmatrix} \tag{17}$$

In the dynamics expression, the acceleration due to to solar radiation $\underline{\mathbf{a}}_{\mathbf{srp}}$ can be considered to be constant and directed only in the x direction with good approximation. On the contrary, the gravitational acceleration due to the small body $\underline{\mathbf{g}}$ is a time-varying term that is strictly connected to the spacecraft position in the Hills frame by a nonlinear relation. To formulate the linearized non-convex terms, the following Jacobians must be computed:

$$\hat{A} = \nabla_x f(\bar{\mathbf{x}},\bar{\mathbf{u}},\bar{p}) = \bar{p}A + \bar{p}\nabla_x\bar{\mathbf{g}} \tag{18a}$$
$$\hat{B} = \nabla_u f(\bar{\mathbf{x}},\bar{\mathbf{u}},\bar{p}) = \bar{p}B \tag{18b}$$
$$\hat{F} = \nabla_p f(\bar{\mathbf{x}},\bar{\mathbf{u}},\bar{p}) = A\bar{\mathbf{x}} + B\bar{\mathbf{u}} + \bar{\mathbf{g}} + \mathbf{a}_{\mathbf{srp}} \tag{18c}$$
$$\hat{r} = f(\bar{\mathbf{x}},\bar{\mathbf{u}},\bar{p}) - \hat{A}\bar{\mathbf{x}} - \hat{B}\bar{\mathbf{u}} - \hat{F}\bar{p} = -(\bar{p}A + \bar{p}\nabla_x\bar{\mathbf{g}})\bar{\mathbf{x}} - \bar{p}B\bar{\mathbf{u}} \tag{18d}$$

so that the convex approximation of the dynamics can be formulated as:

$$\begin{aligned} \dot{\mathbf{x}} &= \hat{A}\mathbf{x} + \hat{B}\mathbf{u} + \hat{F}p + r \\ &= (\bar{p}A + \bar{p}\nabla_x\bar{\mathbf{g}})\mathbf{x} + \bar{p}B\mathbf{u} + (A\bar{\mathbf{x}} + B\bar{\mathbf{u}} + \bar{\mathbf{g}} + \mathbf{a}_{\mathbf{srp}})p + \\ &\quad - (\bar{p}A + \bar{p}\nabla_x\bar{\mathbf{g}})\bar{\mathbf{x}} - \bar{p}B\bar{\mathbf{u}} \end{aligned} \tag{19}$$

The following necessary step to formulate a prediction model suitable for implementation in the convex solver is to select a proper discretization model to switch from a continuous to a discrete time space. The most common choice for these applications is to use a Zero-Order-Hold (ZOH) model for the control, which is assumed to remain constant for each sample k. According to this scheme, the prediction

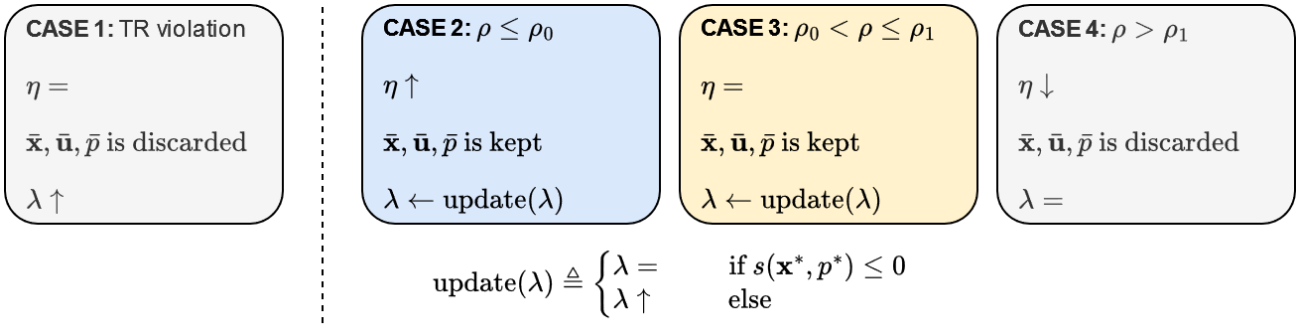

Fig. 6: Visual representation of the GuSTO iterative update procedure.

model to be used for dynamics representation in the equality constraint is formulated as:

$$\begin{aligned} \mathbf{x}_{k+1} = (I_6 + \Delta t\, \bar{p} A + \Delta t\, \bar{p} \nabla_x \bar{\mathbf{g}}) \mathbf{x}_k + \\ + \Delta t\, \bar{p} B \mathbf{u}_k + (A\bar{\mathbf{x}}_k + B\bar{\mathbf{u}}_k + \bar{\mathbf{g}} + \mathbf{a}_{\mathbf{srp}}) \Delta t\, p + \\ - (\Delta t\, \bar{p} A + \Delta t\, \bar{p} \nabla_x \bar{\mathbf{g}}) \bar{\mathbf{x}}_k - \Delta t\, \bar{p} B \bar{\mathbf{u}}_k \end{aligned} \tag{20}$$

It is finally easy to impose firing only around maneuvering points, in order to ensure that the platform is free to perform scientific operations at the pericenter of each hyperbolic trajectory. This is achieved just by imposing $\mathbf{u}_k = \mathbf{0}$ for $k = i, ..., j$ selected at the center of each arc as a simple linear constraint.

4.3 Iterative update rule

As for all SCP algorithms, GuSTO starts from an arbitrary initial guess and relies on an iterative update procedure to converge to the final optimal solution which satisfies the constraints of the problem. This procedure, graphically represented in fig. 6, is thoroughly described in [10], whereas here only a basic description is provided for conciseness. Whenever an iteration takes place, the algorithm checks if the trust region is violated and, if this is the case, it proceeds by discarding the result and increasing the penalty violation coefficient λ. On the other hand, if the solution lies in the trust region, a term $\rho \in (0,1)$ is computed to measure the discrepancy between the nonlinear original problem formulation and the convexified one with respect to the current iteration solution $(\mathbf{x}^*, \mathbf{u}^*, p^*)$:

$$\rho \triangleq \frac{|\mathscr{J}(\mathbf{x}^*, \mathbf{u}^*, p^*) - \mathscr{L}(\mathbf{x}^*, \mathbf{u}^*, p^*)|}{|\mathscr{L}(\mathbf{x}^*, \mathbf{u}^*, p^*)|} \tag{21}$$

where the nonlinear augmented cost $\mathscr{J}(\mathbf{x}^*, \mathbf{u}^*, p^*)$ in the numerator is a temporally discretized version of the nonlinear expression of $L_\lambda(\mathbf{x}, \mathbf{u}, p)$ in Eq.(11). The algorithm then proceeds comparing ρ to two user-defined constants $\rho_0, \rho_1 \in (0,1)$: if $\rho \leq \rho_0$ the convexification accuracy is deemed good, the trajectory is kept and used as the next initial guess, and the trust region can be expanded by a factor β_{gr}; if $\rho_0 < \rho \leq \rho_1$, the convex approximation is still considered satisfactory and the trajectory is stored, but the trust region is kept unchanged; finally, if $\rho > \rho_1$, the convexification not considered reliable, the trajectory is discarded, and the trust region is reduced by a factor β_{sh}. After this first update, a secondary step is needed, since GuSTO convergence relies on the fact that the trust region eventually shrinks to zero [6]. However, when the algorithm starts converging to closer and closer trajectories, the convexification accuracy increases and the trust region instead keeps becoming larger. Therefore, an exponential update is included at the end to ensure that the trust region eventually starts shrinking:

$$\eta \leftarrow \mu^{[1+k-k_*]^+} \eta \tag{22}$$

where $\mu \in (0,1)$ is the exponential shrink coefficient and k_* is a parameter which allows to decide when to stop the exploration phase and start shrinking the trust region.

5. Numerical simulations

5.1 Nominal low-thrust trajectories

First of all, the nominal trajectories for both far and close range have been recomputed using the previously described strategy to remove the impulsive approximation and move to the optimal low-thrust counterpart. This is achieved by keeping the same nominal keypoints to be followed and by enforcing firing only around these keypoints, in order to leave ballistic arcs for scientific operations. The nominal maximum thrust value is 1 mN, with an I_{sp} of 2100 s, in accordance with the technological properties of the currently selected propulsive unit.

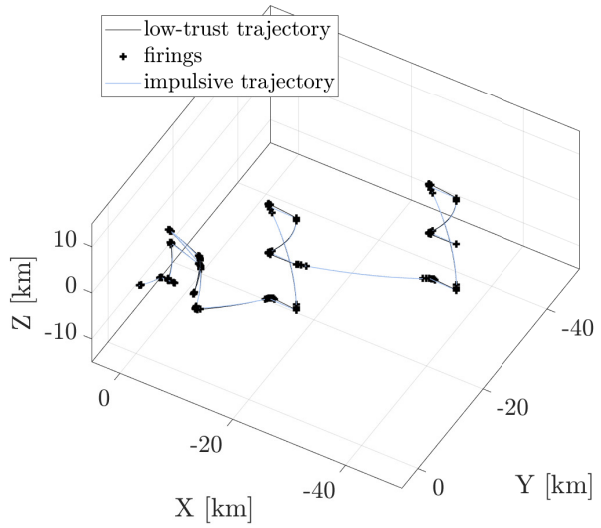

Fig. 7: Low-thrust nominal far range trajectory compared to impulsive solution.

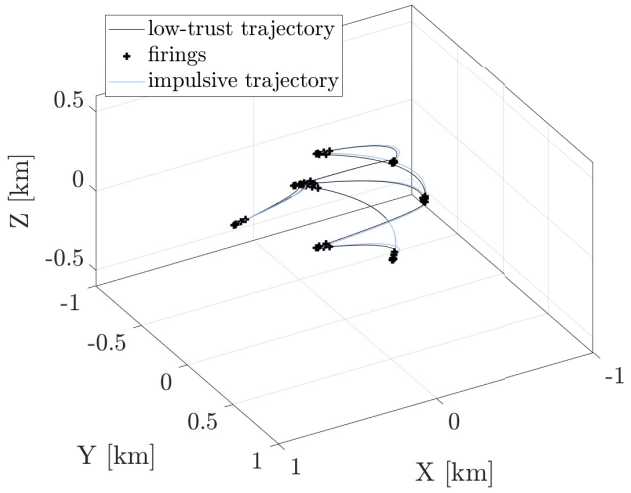

Fig. 8: Low-thrust nominal close range trajectory compared to impulsive solution.

The resulting trajectories are very close to the ones previously obtained with the impulsive approximation. This is mainly due to two reasons: first, the small ΔV necessary to transfer in such a low-gravity environment implies low firing times, secondly, the constraint to fire close to the impulsive firing points ensures that the low-thrust counterpart still maintains the nice scientific properties. This can be observed clearly from fig. 7 and fig. 8, in which the nominal trajectories are represented together.

5.2 Robustness analysis

The robustness of the trajectory design and of the receding horizon controller have been then validated through Monte Carlo (MC) simulations. This evaluation is of paramount importance for the ANIME mission. Indeed, the mass and shape of 2000 SG344 are at the moment known with large uncertainties. In addition, given the large departure window, the heliocentric position of the asteroid and the spacecraft during the rendezvous can vary a lot depending on the actual departure and arrival date, resulting in different values of the solar radiation pressure. The following uncertainties have therefore been considered:

- *Asteroid mass*: at the moment the mass of the target is estimated with a high degree of uncertainty, and nominally set to $7 \cdot 10^7$ kg [5]. However, as the mission continues with its development, observations campaign from ground of the target are likely to be organised, to narrow down this estimate while also improving the orbit estimation. Therefore, the initial asteroid mass uncertainty has been (still conservatively) considered to be $6 \cdot 10^6$ kg, with Gaussian distribution. Moreover, during the mission the asteroid mass will be estimated by the flight dynamics, with a degree of uncertainty that is considered to be 5% (1σ). This has been taken into account in the MC simulations, as it will be explained later.

- *Date*: the date span is considered covering an entire year around the foreseen arrival date, with a sample drawn at the beginning of each MC run from a uniform distribution spanning from 1^{st} June 2031 to 1^{st} June 2032.

- *Control action*: uncertainties on the performance of the electric propulsion unit are considered, both in terms of norm and orientation of the thrust vector. The thrust vector magnitude has been assumed to have a Gaussian distribution centered at the nominal control action value with a variance corresponding to 5% of the control magnitude. The thrust misalignment is modeled as a uniform distribution in a cone of 1° of semi-amplitude centered in the nominal control direction.

- *Navigation*: navigation performances are included in the process, in the form of suitable estimates of the uncertainty in spacecraft position and velocity with respect to the target. The assumed values are 10 m (1σ)

for position accuracy and 1 cm/s (1σ) for velocity accuracy.

The pipeline works in closed loop, with the final conditions of each arc that are fed with their navigation uncertainty to the receding horizon controller, to optimise the next segment of the trajectory. In particular, each run of the MC starts with an initialization, generating the asteroid mass sample and reference starting date and setting the starting point of the first arc. Starting from the asteroid mass sample, the estimated gravitational parameter is generated, considering an additional uncertainty. The mass sample will be used for the propagation in the higher fidelity model, while the gravity parameter is what is used by the algorithm to compute the guidance profile, to simulate a difference between model and reality.

Then, the controller is used sequentially on all the arcs of the phase of reference (far range or close range). The following procedure takes place for each arc:

1. Navigation uncertainty is added to the starting condition, obtaining the estimated starting point of the arc.
2. The optimal control problem is solved, computing the nominal guidance profile for the arc with the receding horizon controller detailed in section 4.
3. The nominal guidance profile is perturbed, adding the control action uncertainty. Each of the N-1 segments of the guidance profile is perturbed with the thrust misalignment and module uncertainty.
4. The trajectory is repropragated in the higher fidelity model, with the perturbed guidance profile.
5. The starting condition is updated, as the final state of the propagation.

The MC simulation has been carried out for both phases of the proximity operations, with 500 samples per phase. Results are reported in the following.

5.2.1 Results - Far range

All the obtained trajectories for the MC simulation of this phase are presented in fig. 9. It is clear to see that there are no major offsets with respect to the nominal trajectory. Compliance with the scientific requirements has also been checked for all the samples and is reported in fig. 10, which is obtained by overlapping the evolution of the SPA and distance of all the samples to the nominal values in fig. 2, fig. 10. The plot shows the robustness of the design of the Far Range proximity operations of the ANIME mission. Looking at the distribution of the ΔV of the samples in fig. 11 it can be noticed that as expected there is an increase in the ΔV cost with respect to the nominal bi-impulsive arc sequence, as here the manoeuvres are continuous thrusting arcs. The average ΔV value is of 4.1 m/s.

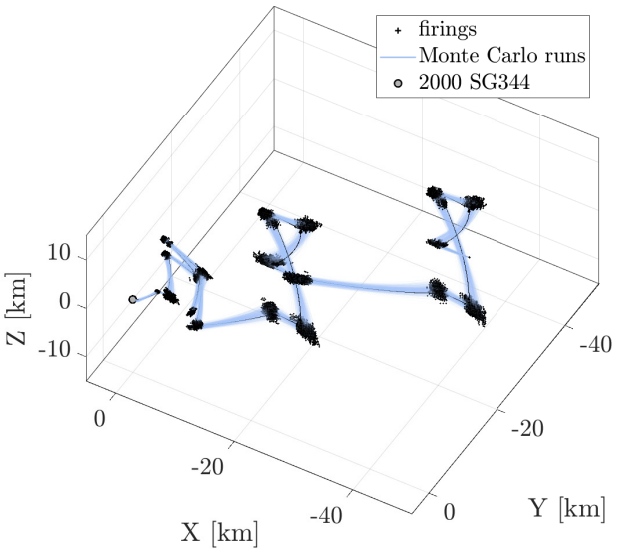

Fig. 9: Trajectory and thruster firings in the far range Monte Carlo simulation.

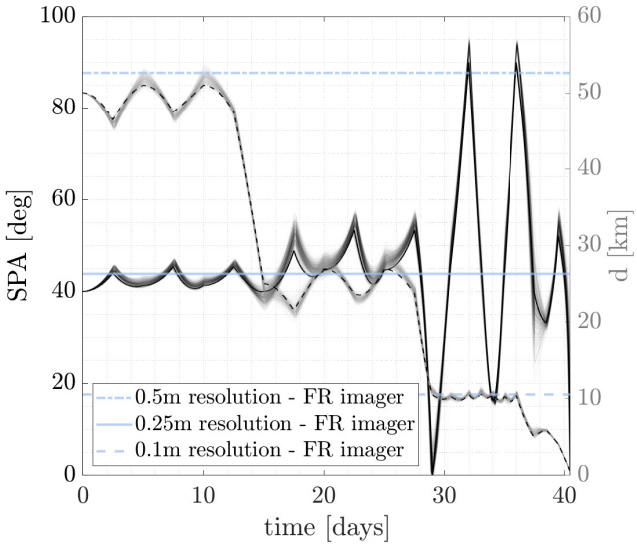

Fig. 10: Sun-Phase Angle and distance evolution in the Far Range Monte Carlo simulation.

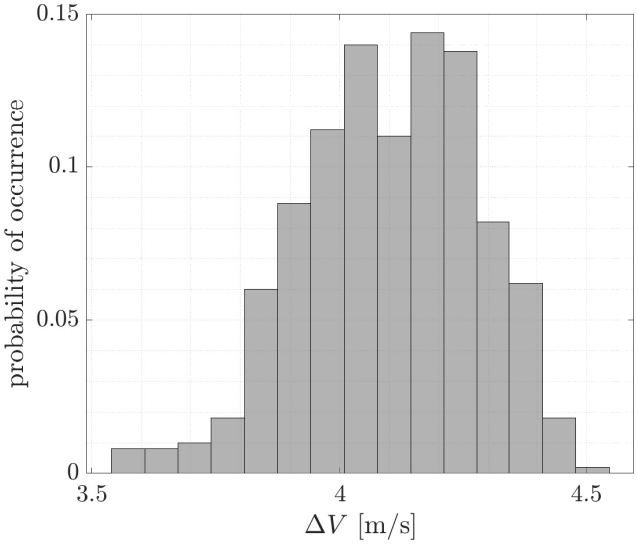

Fig. 11: ΔV distribution for Far Range operations in Monte Carlo simulation.

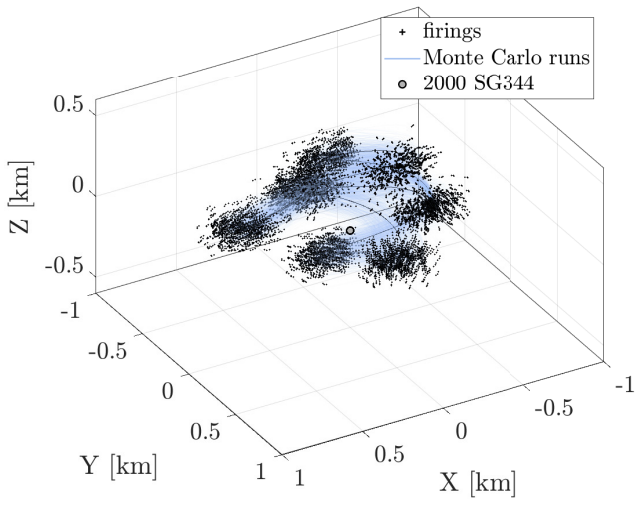

Fig. 12: Trajectory and thruster firings in the Close Range Monte Carlo simulation.

5.2.2 Results - Close range

The Close Range simulations show high robustness to the variables of the problem too, although a much higher variability is observed due to the higher influence of the mass of the asteroid on the dynamics of the spacecraft. The evolution of the 500 simulated trajectories is shown in fig. 12, together with the location of the thruster firings that link the ballistic hyperbolic arcs. A value of 200 m is chosen as the radius of the spherical Keep Out Zone that is used as non-convex path constraint. The satisfaction of the constraint is visible more clearly in fig. 13, in which the distance from the center of mass of the asteroid and the Sun-Phase Angle are shown for each Monte Carlo sample with respect to the nominal trends which have been shown previously in fig. 4. From this figure, it is also visible how all the samples correctly satisfy the scientific objectives of the close-range observation phase, once again showing the robustness of the proposed strategy.

6. Conclusions

This paper shows the results of the proximity mission analysis of ANIME mission, aimed at investigating the asteroid 2000 SG344. The trajectory design, leveraging hyperbolic arcs linked by optimal low-thrust control actions, successfully meets the scientific objectives of the mission of close-range and far-range measurements using optical and radio-science payloads while optimizing fuel consumption over the proximity operations through a single-shooting algorithm and refining the results with Sequential Convex Programming. Furthermore, Monte Carlo analyses are carried out to validate the robustness of the mission trajectory against platform limitations and environmental uncertainties that take into account the extremely wide range of possibilities for the arrival date at the small body. The results confirm that the trajectory design is sufficiently robust to all the

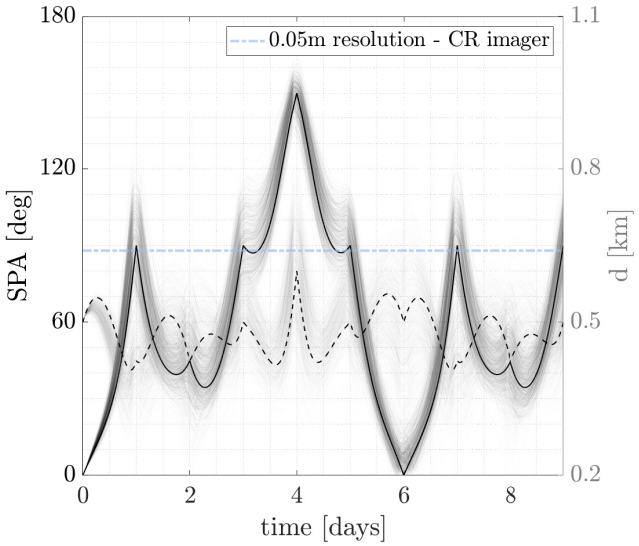

Fig. 13: Sun-Phase Angle and distance evolution in the Close Range Monte Carlo simulation.

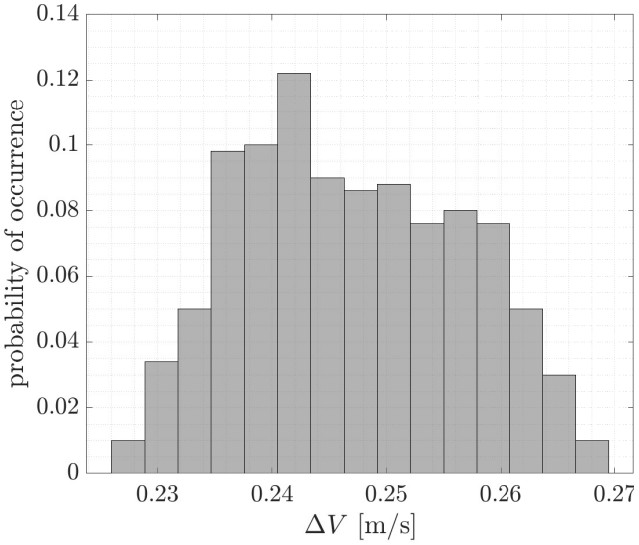

Fig. 14: ΔV distribution for Close Range operations in Monte Carlo simulation.

considered variables of the problem, while successfully satisfying the scientific objectives of ANIME.
For future developments the analysis will be refined, going towards an actual on board implementation of the controller. The first step will be to swap the navigation performance model with an actual simulated navigation architecture, with a navigation filter that estimates the state of the spacecraft using Line Of Sight (LOS) information coming from simulated images and sensor measurements. In addition, periodic updates of range and range rate information will be added, to simulate the navigation information computed by the flight dynamics team and uploaded through contacts with the ground stations. Then, the obtained pipeline will be tested again with Model-In-the-Loop and next, after automatic generation of the validated GNC embeddable code, in Software and then Hardware-in-loop simulations.

7. Acknowledgements

The work presented in this paper was carried out during the Phase A of ANIME project, funded by ASI in the framework of the ALCOR program. The authors would also like to acknowledge the other members of the ANIME consortium, namely, INAF OAR (prime contractor), INAF OAPd, Politecnico di Torino, and Università di Bologna.

References

[1] T. J. Martin-Mur and B. Young, "Navigating marco, the first interplanetary cubesats," in *Proceedings of the 18th Australian International Aerospace Congress, Melbourne, Australia*, 2019, pp. 24–28.

[2] E. Scarpa, N. Battezzati, S. Ciaglia, *et al.*, "The first-ever asteroid fly-by performed by a cubesat: Outcomes of the liciacube mission," 2023.

[3] H. R. Goldberg, Ö. Karatekin, B. Ritter, *et al.*, "The juventas cubesat in support of esa's hera mission to the asteroid didymos," 2019.

[4] T. Kohout, M. Cardi, A. Näsilä, E. Palomba, and F. Topputo, "Milani cubesat for esa hera mission," in *European Planetary Science Congress*, 2021, EPSC2021–732.

[5] NASA-JPL. "Nasa jpl small body database lookup." (), [Online]. Available: https://ssd.jpl.nasa.gov/tools/sbdb_lookup.html#/.

[6] R. Bonalli, A. Cauligi, A. Bylard, and M. Pavone, "Gusto: Guaranteed sequential trajectory optimization via sequential convex programming," May 2019, pp. 6741–6747. DOI: 10.1109/ICRA.2019.8794205.

[7] D. Scheeres, "Orbital mechanics about small bodies," *Acta Astronautica*, vol. 72, pp. 1–14, 2012, ISSN: 0094-5765. DOI: https://doi.org/10.1016/j.actaastro.2011.10.021. [Online]. Available: https://www.sciencedirect.com/science/article/pii/S0094576511003237.

[8] NASA-JPL. "Spice naif toolkit." (), [Online]. Available: https://naif.jpl.nasa.gov/naif/index.html.

[9] NASA-JPL. "Nasa jpl horizons system." (), [Online]. Available: https://ssd.jpl.nasa.gov/horizons/app.html#/.

[10] D. Malyuta, T. P. Reynolds, M. Szmuk, *et al.*, "Convex optimization for trajectory generation: A tutorial on generating dynamically feasible trajectories reliably and efficiently," *IEEE Control Systems Magazine*, vol. 42, no. 5, pp. 40–113, 2022. DOI: 10.1109/MCS.2022.3187542.